

Flavor Symmetry and Ferroelectric Nematics in Transition Metal Dichalcogenides

Patrick Cheung, Zhi-qiang Bao, and Fan Zhang*

Department of Physics, The University of Texas at Dallas, Richardson, TX 75080, USA

Recent magneto-transport experiments have provided compelling evidence for the presence of an energetically isolated threefold Q -valley degeneracy in few-layer transition metal dichalcogenides. We study the flavor $SU(3)$ symmetry breaking when each Landau level triplet is one-third filled or empty and predict that a pure flavor nematic phase and a flavorless charge-density-wave phase will occur respectively below and above a critical magnetic field. Surprisingly, electrons carry flavor-dependent electric dipole moments even at zero magnetic field, rendering the nematics ferroelectric, allowing electric-field manipulation of the flavors, and leading to the concept of flavortronics.

Introduction.—Spontaneous symmetry breaking associated with the internal degrees of freedom of electrons plays a central role in determining the electromagnetic phenomena in materials. Prime examples are charge $U(1)$ symmetry breaking in superconductors and spin $SU(2)$ symmetry breaking in ferromagnets. $SU(2)$ symmetries are also innate to double-layer and dual-valley systems such as few-layer graphene and transition metal dichalcogenides (TMDs) [1–3]. However, flavor $SU(3)$ symmetry appears to be rare in electron systems, although historically it provides a foundation for the quark model [4]. This fact prevents the emergence of novel electromagnetic phenomena that arise from the flavor symmetry or its breaking. Recently, experiments [5–9] have provided compelling evidence for the presence of an energetically isolated threefold Q -valley degeneracy in few-layer TMDs including MoS_2 , $MoSe_2$, WS_2 , and WSe_2 . From this perspective, the TMDs offer an unprecedented platform for exploring the flavor $SU(3)$ symmetry of electrons. (The surface of Bi or SnTe [10–15] also hosts triply degenerate valleys, yet they coexist with other ones that cannot be removed from Fermi energy.)

At the conduction-band edge of a few-layer TMD, there are six inequivalent Q/Q' valleys inside the first Brillouin zone (BZ), as depicted in Fig 1a. The three Q valleys are related by a C_3 symmetry, and the Q and Q' valleys are related by time-reversal (\mathcal{T}) and inversion (\mathcal{P}) symmetries. In an odd-layer system, because of the intrinsic \mathcal{P} asymmetry and strong spin-orbit couplings, the bands are spin split. The z -component of spin is a good quantum number due to the mirror symmetry with respect to the middle metal layer. Thus, the Q -valley bands exhibit both spin splitting and spin-valley locking. In an even-layer system, the restored \mathcal{P} symmetry and the \mathcal{T} symmetry leads to Kramers degeneracy for all the states. As a result, the bands are spin degenerate in each Q valley. Such universal even-odd layer-dependent valley degeneracies have been clearly observed in the Shubnikov-de Hass oscillations [5–7]. At small magnetic fields and low electron densities, the oscillations display a 6 (12) fold Landau level (LL) degeneracy in the odd- (even-) layer systems due to the $C_3 \times \mathcal{T}$ ($C_3 \times \mathcal{T} \times \mathcal{P}$) symmetry. At large fields, the inter- (intra-) valley Zeeman effect

reduces the degeneracy to 3 (6).

Therefore, at magnetic fields $\gtrsim 5$ T and electron densities $\lesssim 10^{13}$ cm $^{-2}$ [5], all the TMD odd-layers thicker than bilayer and the even-layers with an interlayer electric field (to break the \mathcal{P} symmetry) exhibit LL triplets. Because of the similarity to the quark model, and to distinguish from the Q/Q' valley pseudospin, it is proper to label the three degenerate Q valleys of orientations $\theta_f \in \{0, 2\pi/3, 4\pi/3\}$ by their *flavors* $f \in \{u, d, s\}$ as in Fig. 1a. In this unique platform, we examine the interplay between the flavor $SU(3)$ symmetry and electron-electron interactions, by focusing on the case in which the highest LL triplet is 1/3 filled or empty to produce an integer quantum Hall effect. When only the flavor-conserving long-range interactions are retained, the C_3 symmetry is spontaneously broken to yield a nematic state in which all the electrons have the same flavor. When the much weaker flavor-mixing short-range interactions are taken into account, the translational symmetry is lowered beyond a critical magnetic field to create incommensurate charge-density-wave (CDW) states that establish coherence among three flavors. Remarkably, the large effective mass of TMD electrons substantially magnifies the interaction effects, and the lack of inversion centers of Q -valleys renders the nematics ferroelectric. This electronic ferroelectricity [16–18] differs fundamentally from the structural one [19–22]. Interestingly, an in-plane electric field couples to the electron flavor through its flavor-dependent electric dipole moment that survives even at zero magnetic field, thereby tuning the ferroelectric nematics, CDW states, and their competition.

Model.—Near the energy minima ($\mathbf{k} = 0$) of the lowest conduction sub-band of a TMD few-layer, the most general flavor-dependent Q -valley Hamiltonians read

$$H_u(\mathbf{k}) = \frac{\hbar^2 k_x^2}{2m_x} + \frac{\hbar^2 k_y^2}{2m_y} + \frac{\delta_x a \hbar^2 k_x^3}{m_e}, \quad (1)$$

$H_d = C_3 H_u C_3^{-1}$, and $H_s = C_3^{-1} H_u C_3$. Here m_e is the bare electron mass, and a is the lattice constant, e.g., 3.160 Å for MoS_2 . The energy dispersions are nearly quadratic, with different effective masses m_x and m_y along and perpendicular to the ΓK direction, respectively. While each Q valley is symmetric with respect

to its axis ΓK , there is an asymmetry along it, and δ_x characterizes this weak distortion in Eq. (1). These band parameters can be extracted from first-principles calculations, and $\sqrt{m_x m_y}$ can alternatively be obtained from temperature-dependent SdH oscillations [5–7]. Note that their values crucially depend on the layer number. For trilayer MoS₂, our first-principles calculations yield $m_x = 0.594m_e$, $m_y = 0.788m_e$, and $\delta_x = 0.050$, as fitted in Fig. 1b. We ignore the tiny δ_x when deriving the LLs and the broken symmetry states yet treat it perturbatively when computing the electric polarization.

Under a uniform perpendicular magnetic field B_\perp , $\hbar\mathbf{k}$ are replaced by $\boldsymbol{\pi} = \hbar\mathbf{k} + e\mathbf{A}$ with $\mathbf{A} = (0, -B_\perp x)$ in the Landau gauge. Since $[\pi_x, \pi_y] = i\hbar^2/\ell^2$ with $\ell = \sqrt{\hbar/eB_\perp}$ being the magnetic length, we construct a set of raising operators $a_f^\dagger = (\ell/\sqrt{2}\hbar)(\alpha_f\pi_x - i\beta_f\pi_y)$, where $\alpha_f = \eta \cos \theta_f + i\eta^{-1} \sin \theta_f$, $\beta_f = \eta^{-1} \cos \theta_f + i\eta \sin \theta_f$, and $\eta = (m_y/m_x)^{1/4}$. This flavor-dependent construction is necessary, given the *anisotropic* dispersions and *nonparallel* orientations of Q valleys (Fig. 1a). In this representation, $H_f = (a_f^\dagger a_f + 1/2)\hbar\omega$ with $\omega = eB_\perp/\sqrt{m_x m_y}$. The LL energies and wave functions are

$$\begin{aligned} E_{fX}^{(n)} &= (n + 1/2)\hbar\omega, \quad n \in \{0, \mathbb{N}\}, \quad f \in \{u, d, s\}, \\ \Psi_{fX}^{(n)} &= e^{i\mathbf{Q}_f \cdot \mathbf{r}} L_y^{-1/2} e^{ik_y y} N_{fn}^{-1} e^{-\alpha_f \beta_f^* \xi_f^2/2} H_n(\xi_f), \end{aligned} \quad (2)$$

where $X = k_y \ell^2$ are the guiding centers, \mathbf{Q}_f are the valley positions in the BZ, L_y is the system size along \hat{y} , $N_{fn} = (2^n n! \sqrt{\pi} |\alpha_f| \ell)^{1/2}$ are normalization factors, $H_n(\xi_f)$ are Hermite polynomials, and $\xi_f = (x - X_f)/|\alpha_f| \ell$. The LLs of an odd-layer system is plotted in Fig. 1c: each level is triply degenerate due to the flavor symmetry, and quantum Hall effects occur at filling factors $\nu = 3N$ ($N \in \mathbb{N}$). Note that the Zeeman splitting is larger than $\hbar\omega$ for $g^* m_{x,y} > 2m_e$, and that under an electric field the sextets in even-layer systems also split into triplets.

Flavor symmetry breaking.—Now we study the interaction effects at the integer filling factors $\nu = 3N - 2$ and $3N - 1$, i.e., the highest LL triplet is 1/3 filled or empty. We examine whether the emergent flavor symmetry and/or any other crystal symmetry is spontaneously broken and whether the broken symmetry states have charge excitation gaps that produce strong quantum Hall effects. Broken flavor symmetry ground states are either Ising-like or XY-like, as illustrated in Figs. 1d-1g. For an Ising-like state, imbalanced flavor populations are energetically favored. In the extreme limit, it can be a pure flavor state, i.e., $|u\rangle$, $|d\rangle$, or $|s\rangle$. For an XY-like state, coherence among the flavors is spontaneously established. In the symmetric case, it can be a flavorless state such as $|u\rangle + |d\rangle + |s\rangle$. Markedly, the Ising-like states are nematics [24–27], which break the C_3 symmetry, whereas the XY-like states are incommensurate CDW states which lower the translational symmetry.

We employ a Hartree-Fock theory [28–30] to evaluate the interaction effects. The $\nu = 3N - 1$ and $3N - 2$

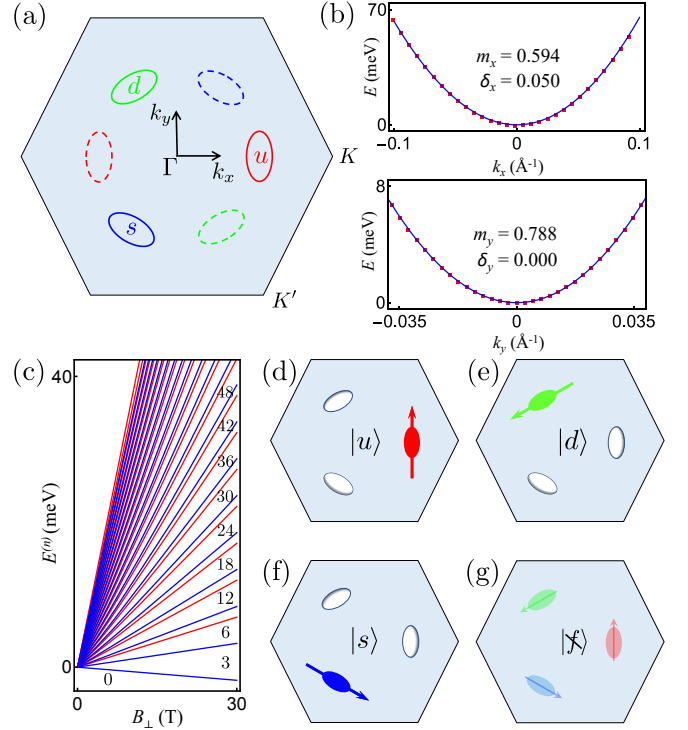


FIG. 1. (a) Schematic of the first BZ of few-layer TMDs. The conduction band minima are located at the six Q (solid) and Q' (dashed) valleys. When both \mathcal{T} and \mathcal{P} symmetries are broken, each Q -valley LL triplet (u, d, s) has an emergent flavor SU(3) symmetry, analogous to the quark model. (b) Band parameter values in Eq. (1) for trilayer MoS₂ extracted from the first-principles calculations (squares). (c) Single-particle LL structure [23] of (b) with $g^* = 5$. The Q (blue) and Q' (red) LL triplets have opposite spins and Zeeman split, yielding quantum Hall states at $\nu = 3N$ ($N \in \mathbb{N}$). (d)-(g) Schematics of interaction-driven broken flavor symmetry states at $\nu = 3N - 2$. The pure flavor states, i.e., $|u\rangle$, $|d\rangle$, and $|s\rangle$, are ferroelectric nematics. The flavorless states, e.g., $|\chi\rangle = (|u\rangle + |d\rangle + |s\rangle)/\sqrt{3}$, are incommensurate CDW states. The color fillings indicate particle populations in the highest triplet, and the arrows depict electric dipole moments.

states are particle-hole symmetric after projecting to the highest LL triplet. This allows us to focus on the $\nu = 3N - 2$ cases. We derive the mean-field Hamiltonians

$$\begin{aligned} H_{ff'}^{(n)} &= E^{(n)}\delta_{ff'} - \sum_{f'' \neq f} U_{ff''}^{(n)} \Delta_{f''f'}^{(n)} \delta_{ff'} \\ &+ W_{ff'}^{(n)} \Delta_{f'f}^{(n)} (1 - \delta_{ff'}) - V_{ff'}^{(n)} \Delta_{f'f}^{(n)}, \end{aligned} \quad (3)$$

where n is the orbital index for the highest LL triplet, $E^{(n)}$ has been given in Eq. (2), and $\Delta_{ff'}^{(n)}$ is the triplet density matrix that must be determined self-consistently. When projected to the subspace of the highest triplet, the flavor-conserving long-range interaction $V_{\mathbf{k}} = 2\pi e^2/\epsilon\mathbf{k}$ and the flavor-mixing short-range scattering $U_Q \sim 2\pi e^2 a/\epsilon$ (with ϵ the dielectric constant) give rise to the Hartree matrix $W_{ff'}^{(n)} = (2\pi\ell^2)^{-1} U_Q F_{ff'}^{nn}(0) F_{ff'}^{nn}(0)$ and

the two exchange (Fock) matrices in Eq. (3)

$$\begin{aligned} V_{ff'}^{(n)} &= \int \frac{d^2\mathbf{k}}{(2\pi)^2} V_{\mathbf{k}} F_{ff}^{nn}(\mathbf{k}) F_{f'f'}^{nn}(-\mathbf{k}) e^{i\varphi_{ff'}^v}, \\ U_{ff'}^{(n)} &= \int \frac{d^2\mathbf{k}}{(2\pi)^2} U_Q F_{ff}^{nn}(\mathbf{k}) F_{f'f'}^{nn}(-\mathbf{k}) e^{i\varphi_{ff'}^u}. \end{aligned} \quad (4)$$

Here $F_{ff'}^{nn}$ is the generalized form factor [31], $\varphi_{ff'}^v = k_x k_y \ell^2 (1 - \varphi_{ff} - \varphi_{f'f'})$, $\varphi_{ff'}^u = k_x k_y \ell^2 (1 - \varphi_{ff} - \varphi_{f'f'})$ with $\varphi_{ff} = \gamma_{ff}^*/(\gamma_f + \gamma_{f'})$ and $\gamma_f = \beta_f/\alpha_f$. If the Q valleys were isotropic, then $\alpha_f, \beta_f, \gamma_f = 1$, $\varphi_{ff'}^v, u = 0$, and $F_{ff'}^{00} = \exp(-k^2 \ell^2/4)$, as in the case of circular cyclotron orbits [28]. Below, the flavor-dependent anisotropy plays an important role in determining the ground states.

The broken flavor symmetry ground state minimizes the total energy of Eq. (3). For the most general trial wave function parametrized as $(c_u e^{i\phi_u}, c_d e^{i\phi_d}, c_s)^T$ with $\sum_f c_f^2 = 1$, the relative total energy per electron reads

$$\bar{E}_T^{(n)} = \left[V_S^{(n)} - V_D^{(n)} + W_D^{(n)} - U_D^{(n)} \right] \sum_{f \neq f'} c_f^2 c_{f'}^2. \quad (5)$$

Because of the charge conservation of each flavor, $\bar{E}_T^{(n)}$ does not depend on the phases ϕ_u and ϕ_d ; yet ground states break these symmetries. The second factor in Eq. (5) is minimized by the three pure flavor states $|u\rangle = (1, 0, 0)^T$, $|d\rangle = (0, 1, 0)^T$, and $|s\rangle = (0, 0, 1)^T$, whereas it is maximized by those flavorless states $(e^{i\phi_u}, e^{i\phi_d}, 1)^T/\sqrt{3}$. Thus, the sign of the first factor in Eq. (5) determines the nature of ground states. Because of the flavor symmetry, the flavor-conserving exchange matrix has two inequivalent elements, the diagonal $V_S^{(n)}$ for electrons of the same flavor and the off-diagonal $V_D^{(n)}$ for electrons of different flavors. By contrast, the flavor-mixing matrices only have the off-diagonal elements $U_D^{(n)}$ and $W_D^{(n)}$ for electrons of different flavors.

Exchange energies are stronger between LL orbitals that are more similar. It follows that for the flavor-conserving interaction $V_S^{(n)} - V_D^{(n)} > 0$ in Eq. (5), given the flavor-dependent anisotropy of Q valleys. This fact favors a nematic ground state $|u\rangle$, $|d\rangle$, or $|s\rangle$ that has a pure flavor, when the much weaker flavor-mixing scattering U_Q can be ignored. While $V_S^{(n)} - V_D^{(n)}$ is positive and scales as $e^2/\ell \sim \sqrt{B_\perp}$, $W_D^{(n)} - U_D^{(n)}$ is negative and scales as $e^2 a/\ell^2 \sim B_\perp$. Despite $a < \ell = 25.6/\sqrt{B_\perp[\text{T}]} \text{ nm}$, at sufficiently large fields the short-range U_Q dominates to favor the CDW states such as the flavorless $|u\rangle + |d\rangle + |s\rangle$. Taking $U_Q = 2\pi e^2 s a/\epsilon$ ($\epsilon \simeq 20$), we find the first order transition at $B_\perp^c = 1454/s^2 \text{ T}$ for the $n = 0$ triplet.

Ferroelectricity.—For a pure flavor nematic state, all the electrons at Fermi energy are confined in one Q valley. This valley is located at a non time-reversal-invariant momentum and lacks an inversion center. For the flavor u in Fig. 1a, the parameter δ_x in Eq. (1) characterizes the band distortion along \hat{x} . In light of a recent theory on

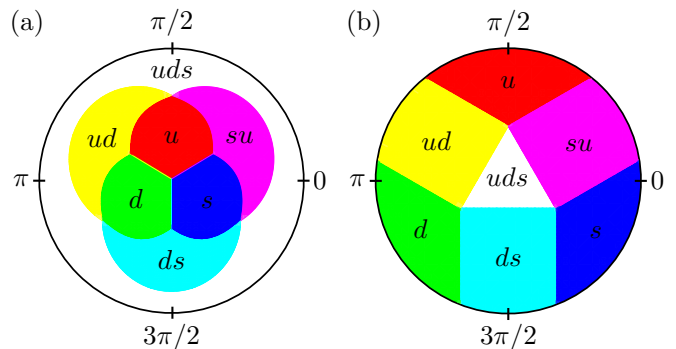


FIG. 2. Phase diagrams at $\nu = 1$ versus the field strengths (radial) and the orientation of E_{\parallel} (angular). (a) B_{\perp} varies from 0 to 40 T at $E_{\parallel} = 1.5 \text{ mV}\cdot\text{nm}^{-1}$. (b) E_{\parallel} varies from 0 to 2.0 $\text{mV}\cdot\text{nm}^{-1}$ at $B_{\perp} = 20 \text{ T}$. $f \in \{u, d, s\}$ label the pure flavor ferroelectric nematics; ff' and uds label the two- and three-flavor coherent states with generally unequal flavor populations. The lines at $\theta = 3\pi/2 - \theta_f$ in (a) are first order transitions between different pure flavor states; all other lines are continuous transitions between states with coherence among different number of flavors. We have chosen $s = 10$.

quantum Hall ferroelectrics [16], the state $|u\rangle$ must carry an electric dipole moment along \hat{y} . In the Berry phase approach to polarization [32–35], the electric dipole moment per electron reads

$$p_u^{(n)} = -\frac{e}{L_x} \int_0^{L_x} \langle u_{uX}^{(n)} | i\nabla_{k_y} | u_{uX}^{(n)} \rangle dX, \quad (6)$$

where L_x is the system size along \hat{x} , and $|u_{uX}^{(n)}\rangle$ is the cell periodic eigenstate for $k_y = X/\ell^2$. By applying the $x - k_y \ell^2$ dependence of $u_{uX}^{(n)}(x)$ to Eq. (6), we obtain

$$p_u^{(n)} = e\ell^2 \int_{-\infty}^{+\infty} u_{u0}^{(n)*}(x) i\nabla_x u_{u0}^{(n)}(x) dx. \quad (7)$$

For the undistorted case, $u_{u0}^{(n)}(x)$ is the wave function in Eq. (2) but without the first three factors. Because of the definite parity of $u_{u0}^{(n)}(x)$, Eq. (7) vanishes as expected. For the distorted case, by employing the perturbation theory to the $2M$ -th order, we find

$$p_u^{(n)} = \sum_{m=1}^M C_{2m-1} \left(\frac{\delta_x a}{\ell} \right)^{2m-1} e\ell, \quad (8)$$

where C_{2m-1} are dimensionless coefficients and $C_{2m} = 0$. Evidently, the dipole moment per electron scales with B_{\perp}^{m-1} perturbatively at the $(2m-1)$ -th order; the leading order does not depend on B_{\perp} and must survive even at $B_{\perp} = 0$. As the distortion has larger effects at higher energies, the higher the LL index n , the larger the $p_u^{(n)}$. For the $n = 0$ triplet, we obtain at the leading order

$$p_u^{(0)} = \frac{m_x}{m_y} \frac{\sqrt{m_x m_y}}{m_e} \frac{3\delta_x}{2} ea. \quad (9)$$

This produces a dipole moment $0.04ea$ per electron for trilayer MoS₂, which amounts to a polarization density $5.0B_{\perp}[\text{T}] \times 10^{-4} \text{ pC}\cdot\text{m}^{-1}$, given that the electron density per Landau level is $1/2\pi\ell^2$. For comparison, the recently discovered 2D ferroelectric materials have polarization densities [19–22] of $10 - 100 \text{ pC}\cdot\text{m}^{-1}$. Whereas these 2D materials are structural ferroelectrics, the ferroelectricity of our quantum Hall nematics is an electronic property emergent from spontaneous symmetry breaking in a dilute electron gas, i.e., ~ 1 electron per 2000 sites at $B = 20 \text{ T}$ (or $a^2/2\pi\ell^2$). In this sense, our obtained dipole moment per electron is reasonable and large.

Electric field effect.—As a result, an electron in the n -th LL of flavor f carries an in-plane dipole moment $p_f^{(n)} = p_u^{(n)}$ at an angle of $\pi/2 + \theta_f$ from the x -axis. This implies that an in-plane electric field E_{\parallel} couples to the nematic order parameters by breaking the C_3 symmetry and influences the flavor ordering by producing flavor-dependent electrostatic energies

$$\delta E_f^{(n)} = -p_f^{(n)} E_{\parallel} \cos\left(\theta_f + \frac{\pi}{2} - \theta\right), \quad (10)$$

where θ is the in-plane orientation angle of E_{\parallel} from the x -axis. It follows that $E^{(n)} \rightarrow E^{(n)} + \delta E_f^{(n)}$ in Eq. (3). In the absence of interactions, the E_{\parallel} field lifts the triplet degeneracies, favors pure flavor states, and creates integer quantum Hall effects at $\nu = 3N - 2$ and $3N - 1$ except for several special orientations. For $\theta = 3\pi/2 - \theta_f$, there is still a twofold degeneracy at $\nu = 3N - 2$, and likewise for $\theta = \pi/2 + \theta_f$ at $\nu = 3N - 1$.

The electrostatic energies compete with the electron-electron interactions by adding $\sum_f c_f^2 \delta E_f^{(n)}$ to Eq. (5). This greatly enriches the phase diagrams. Figure 2a displays a typical phase diagram at $\nu = 1$ ($n = 0$) for $E_{\parallel} = 1.5 \text{ mV}\cdot\text{nm}^{-1}$. Below the B_{\perp}^c derived above, interactions favor a pure flavor nematic state, and θ selects the flavor, with first order transition lines at $\theta = 3\pi/2 - \theta_f$. Above B_{\perp}^c , as interactions prefer to mix flavors, and electrostatic energies stabilize two-flavor and three-flavor coherent states with generally unequal flavor populations that are continuously tunable by the two fields. These features are also exhibited by Fig. 2b at a fixed $B_{\perp} > B_{\perp}^c$. If E_{\parallel} is smaller in Fig. 2a, the critical points at $3\pi/2 - \theta_f$ remain B_{\perp}^c whereas those at $\pi/2 + \theta_f$ move closer to B_{\perp}^c , and the space for the two-flavor states shrinks. Note that B_{\perp}^c would be enhanced for larger Q -valley anisotropy or weaker short-range interactions.

Discussion.—In quantum transport, Hall plateaus and SdH minima at $\nu = 3N \pm 1$ can be strong evidence for the flavor symmetry breaking. The nematic states can be imaged by Scanning Tunneling Spectroscopy via impurity scattering [12] and probed by measuring the anisotropy in optical conductivity or dielectric function. All these signatures are highly sensitive to the external fields $E_{\parallel}(\theta)$ and B_{\perp} . It would also be intriguing to explore the Pockels and Kerr electro-optic effects in birefringence, utilize

the hysteresis of nematic ferroelectricity for tunable capacitor and memory functions, and examine the effects of uniaxial strain that breaks the flavor symmetry.

Pure flavor nematic states can be pinned by atomic impurities. As domain walls proliferate thermally above a critical temperature [36–39], the temperature to which the nematics survive is limited by domain wall nucleation. In sharp contrast to many other nematics [24–27], the ones studied here have full bulk gaps and chiral edge states. Thus, the domain walls host counter-propagate edge states when flavor-mixing scattering is negligibly weak [40–45]. Moreover, the emergent ferroelectricity enables manipulation of the domain walls by external fields such as $E_{\parallel}(\theta)$ and B_{\perp} , as showcased in Fig. 2.

The quantum Hall nematicity and electric polarization density are continuously tunable by $E_{\parallel}(\theta)$ and B_{\perp} fields (Fig. 2). The dipole moment of a given flavor is reversed by reversing the B_{\perp} field. Yet, this also switches from the Q to Q' valleys (Fig. 1a) that have opposite spin splittings and band distortions. Thus, the measured polarization is not expected to reverse. Finally, the fact that the leading contribution to the dipole moment per electron in Eq. (8) is independent of B_{\perp} implies the existence of flavor-dependent dipole moments at $B_{\perp} = 0$. Therefore, while the out-of-plane orientation of Zeeman field selects the locked spin and valley, the in-plane orientation of electric field selects the flavor of electrons, giving rise to a new concept: the flavortronics.

Acknowledgement.—We thank Philip Kim, Allan MacDonald, Kin Fai Mak, Joe Qiu, Ning Wang, and Emanuel Tutuc for helpful discussions. We are grateful to Xiao Li and Gui-Bin Liu for technical help.

* zhang@utdallas.edu

- [1] A. H. Castro Neto, F. Guinea, N. M. R. Peres, K. S. Novoselov, and A. K. Geim, *The electronic properties of graphene*, *Rev. Mod. Phys.* **81**, 109 (2009).
- [2] X. Xu, W. Yao, D. Xiao, and T. F. Heinz, *Spin and pseudospins in layered transition metal dichalcogenides*, *Nat. Phys.* **10**, 343 (2014).
- [3] K. F. Mak and J. Shan, *Photonics and optoelectronics of 2D semiconductor transition metal dichalcogenides*, *Nature Photonics* **10**, 216 (2016).
- [4] W. Greiner and B. Müller, *Quantum mechanics: symmetries* (Springer-Verlag Berlin Heidelberg, 1994).
- [5] Z. Wu, S. Xu, H. Lu, A. Khamoshi, G.-B. Liu, T. Han, Y. Wu, J. Lin, G. Long, Y. He, Y. Cai, Y. Yao, F. Zhang, and Ning Wang, *Even-odd layer-dependent magnetotransport of high-mobility Q-valley electrons in transition metal disulfides*, *Nat. Commun.* **7**, 12955 (2016).
- [6] R. Pisoni, Y. Lee, H. Overweg, M. Eich, P. Simonet, K. Watanabe, T. Taniguchi, R. Gorbachev, T. Ihn, and K. Ensslin, *Gate-defined one-dimensional channel and broken symmetry states in MoS₂ van der Waals heterostructures*, *Nano Lett.* **17**, 5008 (2017).
- [7] Q. H. Chen, J. M. Lu, L. Liang, O. Zheliuk, A. Ali, P.

- Sheng, and J. T. Ye, *Inducing and manipulating hetero-electronic states in a single MoS₂ thin flake*, *Phys. Rev. Lett.* **119**, 147002 (2017).
- [8] K. Wang, K. De Greve, L. A. Jauregui, A. Sushko, A. High, Y. Zhou, G. Scuri, T. Taniguchi, K. Watanabe, M. D. Lukin, H. Park, and P. Kim, *Electrical control of charged carriers and excitons in atomically thin materials*, *Nat. Nano.* **13**, 128 (2018).
- [9] H. Liu, J. Chen, H. Yu, F. Yang, L. Jiao, G.-B. Liu, W. Ho, C. Gao, J. Jia, W. Yao, and M. Xie, *Observation of intervalley quantum interference in epitaxial monolayer tungsten diselenide*, *Nature Comm.* **6**, 8180 (2015).
- [10] L. Li, J. G. Checkelsky, Y. S. Hor, C. Uher, A. F. Hebard, R. J. Cava, and N. P. Ong, *Phase transitions of Dirac electrons in bismuth*, *Science* **321**, 547 (2008).
- [11] Z. Zhu, A. Collaudin, B. Fauqué, W. Kang, and K. Behnia, *Field-induced polarization of Dirac valleys in bismuth*, *Nature Physics* **8**, 89 (2012).
- [12] B. E. Feldman, M. T. Randeria, A. Gyenis, F. Wu, H. Ji, R. J. Cava, A. H. MacDonald, and A. Yazdani, *Observation of a nematic quantum Hall liquid on the surface of bismuth*, *Science* **354**, 316 (2016).
- [13] T. H. Hsieh, H. Lin, J. Liu, W. Duan, A. Bansil, and L. Fu, *Topological crystalline insulators in the SnTe material class*, *Nat. Commun.* **3**, 982 (2012).
- [14] Y. Shi, M. Wu, F. Zhang, and J. Feng, *(111) surface states of SnTe*, *Phys. Rev. B* **90**, 235114 (2014).
- [15] X. Li, F. Zhang, and A. H. MacDonald, *SU(3) quantum Hall ferromagnetism in SnTe*, *Phys. Rev. Lett.* **116**, 026803 (2016).
- [16] I. Sodemann, Z. Zhu, and L. Fu, *Quantum Hall ferroelectrics and nematics in multivalley systems*, *Phys. Rev. X* **7**, 041068 (2017).
- [17] D.-W. Wang, E. Demler, and S. Das Sarma, *Spontaneous symmetry breaking and exotic quantum orders in integer quantum Hall systems under a tilted magnetic field*, *Phys. Rev. B* **68**, 165303 (2003).
- [18] Y. Barlas, R. Côté, K. Nomura, and A. H. MacDonald, *Intra-Landau-level cyclotron resonance in bilayer graphene*, *Phys. Rev. Lett.* **101**, 097601 (2008).
- [19] L. Onsager, *Crystal statistics. I. a two-dimensional model with an order-disorder transition*, *Phys. Rev.* **65**, 117 (1944).
- [20] K. Chang, J. Liu, H. Lin, N. Wang, K. Zhao, A. Zhang, F. Jin, Y. Zhong, X. Hu, W. Duan, Q. Zhang, L. Fu, Q.-K. Xue, X. Chen, and S.-H. Ji, *Discovery of robust in-plane ferroelectricity in atomic-thick SnTe*, *Science* **353**, 274 (2016).
- [21] R. Fei, W. Kang, and L. Yang, *Ferroelectricity and phase transitions in monolayer group-IV monochalcogenides*, *Phys. Rev. Lett.* **117**, 097601 (2016).
- [22] H. W. Wang and X. Qian, *Two-dimensional multiferroics in monolayer group IV monochalcogenides*, *2D Mater.* **4**, 015042 (2017).
- [23] Fig. 1c plots the LLs of the lowest spin-split subbands. The Zeeman splitting is between the opposite spins respectively in the Q and Q' valleys. The LL structure for the next spin-split subbands is almost identical but at a few tens of meV higher in energy, producing LL crossings.
- [24] E. Fradkin, S. A. Kivelson, M. J. Lawler, J. P. Eisenstein, and A. P. Mackenzie, *Nematic Fermi fluids in condensed matter physics*, *Annu. Rev. Condens. Matter Phys.* **1**, 153 (2010).
- [25] S. A. Kivelson, E. Fradkin, and V. J. Emery, *Electronic liquid-crystal phases of a doped Mott insulator*, *Nature* **393**, 550 (1998).
- [26] M. P. Lilly, K. B. Cooper, J. P. Eisenstein, L. N. Pfeiffer, and K. W. West, *Anisotropic states of two-dimensional electron systems in high Landau levels: Effect of an in-plane magnetic field*, *Phys. Rev. Lett.* **83**, 824 (1999).
- [27] R. R. Du, D. C. Tsui, H. L. Stormer, L. N. Pfeiffer, K. W. Baldwin, and K. W. West, *Strongly anisotropic transport in higher two-dimensional Landau levels*, *Solid State Comm.* **109**, 389 (1999).
- [28] R. Côté and A. H. MacDonald, *Collective modes of the two-dimensional Wigner crystal in a strong magnetic field*, *Phys. Rev. B* **44**, 8759 (1991).
- [29] J. Schliemann and A. H. MacDonald, *Bilayer quantum Hall systems at filling factor $\nu = 2$: An exact diagonalization study*, *Phys. Rev. Lett.* **84**, 4437 (2000).
- [30] S. M. Girvin, *Spin and isospin: Exotic order in quantum Hall ferromagnets*, *Physics today* **53**, 39 (2000).
- [31] $F_{ff'}^{nn'}(\mathbf{k}) = N_{fn}^{-1} \cdot N_{f'n'}^{-1} \cdot I \cdot \ell \cdot \exp\left[\frac{k_x^2 \ell^2 + \gamma_f \gamma_{f'} k_y^2 \ell^2}{-2(\gamma_f + \gamma_{f'})}\right]$ where $I = \int_{-\infty}^{+\infty} e^{-\frac{1}{2}(\gamma_f + \gamma_{f'})\zeta^2} \cdot H_n\left(\frac{\zeta + \omega_f}{|\alpha_{f'}|}\right) \cdot H_{n'}\left(\frac{\zeta + \omega_{f'}}{|\alpha_{f'}|}\right) d\zeta$, $\omega_f = \frac{ik_x \ell - \gamma_f^* k_y \ell}{\gamma_f + \gamma_{f'}}$, and $\omega_{f'} = \frac{ik_x \ell + \gamma_f k_y \ell}{\gamma_f + \gamma_{f'}}$.
- [32] J. Zak, *Berry's phase for energy bands in solids*, *Phys. Rev. Lett.* **62**, 2747 (1989).
- [33] R. D. King-Smith and D. Vanderbilt, *Theory of polarization of crystalline solids*, *Phys. Rev. B* **47**, 1651 (1993).
- [34] R. Resta, *Macroscopic polarization in crystalline dielectrics: The geometric phase approach*, *Rev. Mod. Phys.* **66**, 899 (1994).
- [35] D. Xiao, M.-C. Chang, and Q. Niu, *Berry phase effects on electronic properties*, *Rev. Mod. Phys.* **82**, 1959 (2010).
- [36] X. Li, F. Zhang, Q. Niu, and A. H. MacDonald, *Spontaneous layer-pseudospin domain walls in bilayer graphene*, *Phys. Rev. Lett.* **113**, 116803 (2014).
- [37] M. Shayegan, E. P. De Poortere, O. Gunawan, Y. P. Shkolnikov, E. Tutuc, and K. Vakili, *Two-dimensional electrons occupying multiple valleys in AlAs*, *Physica Status Solidi (B)* **243**, 3629 (2006).
- [38] D. A. Abanin, S. A. Parameswaran, S. A. Kivelson, and S. L. Sondhi, *Nematic valley ordering in quantum Hall systems*, *Phys. Rev. B* **82**, 035428 (2010).
- [39] A. Kumar, S. A. Parameswaran, and S. L. Sondhi, *Microscopic theory of a quantum Hall Ising nematic: Domain walls and disorder*, *Phys. Rev. B* **88**, 045133 (2013).
- [40] F. Zhang, *Topological valleytronics: Brought to light*, *Nat. Phys.* **14**, 111 (2018).
- [41] I. Martin, Y. M. Blanter, and A. F. Morpurgo, *Topological confinement in bilayer graphene*, *Phys. Rev. Lett.* **100**, 036804 (2008).
- [42] F. Zhang, A. H. MacDonald, and E. J. Mele, *Valley Chern numbers and boundary modes in gapped bilayer graphene*, *Proc. Natl. Acad. Sci. USA* **110**, 10546 (2013).
- [43] A. Vaezi, Y. Liang, D. H. Ngai, L. Yang, and E.-A. Kim, *Topological edge states at a tilt boundary in gated multi-layer graphene*, *Phys. Rev. X* **3**, 021018 (2013).
- [44] L. Ju, Z. Shi, N. Nair, Y. Lv, C. Jin, J. Velasco Jr, C. Ojeda-Aristizabal, H. A. Bechtel, M. C. Martin, A. Zettl, J. Analytis, and F. Wang, *Topological valley transport at bilayer graphene domain walls*, *Nature* **520**, 650 (2015).
- [45] J. Li, K. Wang, K. J. McFaul, Z. Zern, Y. Ren, K. Watanabe, T. Taniguchi, Z. Qiao, and J. Zhu, *Gate-controlled*

topological conducting channels in bilayer graphene, [Nat. Nanotechnol. 11, 1060 \(2016\)](#).